Alexandria Engineering Journal (2023) 74, 689–704

HOSTED BY

Alexandria University

Alexandria Engineering Journal

www.elsevier.com/locate/aej
www.sciencedirect.com

ORIGINAL ARTICLE

Flexible Sector Detector-Based Mismatch Supply Voltage in Direct Torque Control Doubly Fed Induction Machine: An Experimental Validation

Muhammad Zaid Aihsan [a], Auzani Jidin [b], Muhammad Mokhzaini Azizan [c,*], Muhammad Izuan Fahmi [a], Khairunnisa Hasikin [d]

[a] *Faculty of Electrical Engineering & Technology, Universiti Malaysia Perlis, Arau, Malaysia*
[b] *Faculty of Electrical Engineering, Universiti Teknikal Malaysia Melaka, Durian Tunggal, Malaysia*
[c] *Department of Electrical and Electronic Engineering, Faculty of Engineering and Build Environment, Universiti Sains Islam Malaysia, Nilai, Malaysia*
[d] *Department of Biomedical Engineering, Faculty of Engineering, Universiti Malaya, Kuala Lumpur, Malaysia*

Received 23 December 2022; revised 8 April 2023; accepted 14 May 2023
Available online 26 May 2023

KEYWORDS

Direct Torque Control (DTC);
Open-End Winding;
Induction Machine;
Mismatch voltage;
Dual-Inverter

Abstract Direct Torque Control (DTC) of Induction Motors (IMs) is popular in motor drive applications because of its robust and simple control structure. The IM winding can be controlled on both sides using dual inverter technique which more effective for Electric Vehicle (EV) with a greater number of voltage vectors. However, the battery performance of the dual inverter will deteriorate unevenly on both sides, resulting in fluctuating voltages for the EV system. This will lead to the generation of distorted stator currents and a significant droop in the stator flux, which in turn can increase the total harmonic distortion (THD) in the system. Additionally, the performance of torque may not be able to regulate effectively. This paper examines the effect of unstable voltage on voltage vector mapping performance with tilted angles and proposes new sector definitions based on voltage ratio conditions. Moreover, the proposed sector for each predefined voltage ratio is tested under three-speed conditions. The proposed technique effectiveness is validated through hardware experiments using a dSPACE 1104 controller and retuning the stator current for proper waveform. This approach improves the stator current waveform, improves stator flux droop, enhances torque regulation and minimizes the THD in the DTC system.

1. Introduction

The demand for induction machine (IM) drives in industrial applications is rapidly rising, particularly in Electric Vehicles (EVs) systems due to their robustness and high dynamic per-

* Corresponding author.
E-mail address: mokhzainiazizan@usim.edu.my (M.M. Azizan).
Peer review under responsibility of Faculty of Engineering, Alexandria University.

https://doi.org/10.1016/j.aej.2023.05.060
1110-0168

formance [1]. The IM can be driven by two types of vector control structure, namely Field Oriented Control (FOC) and Direct Torque Control (DTC) [2–4]. The FOC technique refers to the first vector control using the flux vector decomposition technique to enhance the dynamic performance of the induction motor. In FOC, a Proportional Integral (PI) controller is employed to handle the d and q current components required to control torque and flux [5]. To handle the FOC technique, researchers need to know the machine parameters and knowledge of the frame transformation. In addition, it needs immediate position information on the coordinates transformation to determine the proper voltage space vector [6]. In contrast to FOC, the DTC system has better merits as the system has less dependence on the machine parameters but can perform an excellent dynamic torque response [7–10]. The voltage vector can be directly controlled using a pre-design look-up table, and the torque and flux control is based on the hysteresis comparators.

The DTC system proposed by Takahashi and N. Noguchi [10] was based on a hysteresis-based module, and it has an upper band and lower band limit that allow torque to travel within the area. Note that the faulty selection of voltage vector will result in a vigorous and uncontrollable movement of torque that leads to overshoot and undershoot within the hysteresis band, which cause large torque ripple and variable switching frequency, especially during low-speed condition [11]. The stator flux and torque reference information will be injected into the hysteresis controller to produce the required status to be used in the look-up table. In the look-up table, the voltage vectors are arranged according to each stator flux and torque status, producing the switching state for the inverter. Several studies have been done by previous researchers to improve the hysteresis-based technique. One of the easiest methods, known as adjustable hysteresis band size [12,13] uses the technique of modifying the band size to allow precise torque regulation. However, this method is suitable for small sampling rate devices, such as Digital Signal Processor (DSP) controllers, and they require complex hardware arrangement. For example, a DTC system that uses a dSPACE-based controller runs at a minimum sample rate of 50 μs, which might cause the torque to rapidly travel between the upper and lower bands, leading to overshoot and undershoot unconditionally and causing variable switching frequency conditions [14,15]. Another approach using two dynamic hysteresis bands is reported in [16], where this strategy is to encounter poor flux regulation during low-speed operation. It is done by altering the amplitude of the hysteresis torque band by looking at the flux error range.

In recent years, a wide range of studies focused on inverter topology structures to improve the DTC performance in IM. The standard two-level inverter is now replaced by the multilevel inverter concept as it generates a significant amount of voltage vector, which is very helpful in improving the better control of stator flux and torque of IM [17–20]. There are several types of multilevel inverters in the DTC system, namely as three-level neutral point clamp (NPC), flying capacitor (FC), cascaded H-bridge (CHB), and the dual inverter technique using open-end winding configurations [21–25]. For the NPC and FC topology, it drives the IM using single-ended operation, which is highly dependent on the inverter and DC supply voltage. If the inverter or DC voltage supply is damaged, the IM will fully stop its operation [26,27], which is not practical for real-time drive systems such as EV applications. In contrast to CHB and the dual inverter technique, it applies several isolated DC link supplies to power up the IM. If any faulty power supplies occur, it still allows the whole system to be operated, but in lower power, the stator current will face some disturbance. Thus, it leads to the increment in harmonic stator currents [28,29]. Furthermore, the disturbance in the stator current might cause the torque performance not to be regulated [30].

With this direction and motivation, this paper attempts to address the issue of distorted stator current during the imbalance supply from the battery to the dual inverter. In the Direct Torque Control Open Ended Winding Induction Machine (DTC-OEWIM), an active voltage vector is formed by the resultant voltage vector between inverter 1 and inverter 2. Usually, the angle of the resultant voltage vector formed in the balanced voltage supply is aligned and tangential to the default flux sector definitions. However, when the supplied voltage is unequal or imbalanced, the angle of the resultant voltage vector formed will be tilted and does not align or tangential to the default flux sector definitions. Apart from that, the higher voltage difference between the dual inverter will result in a wider angle of the resultant vector to be tilted.

To cater to this circumstance, a new sector definitions is designed to meet the requirements of the new resultant voltage vector pattern. The implementation involves examining the characteristics of the resulting voltage vector for each predetermined voltage ratio between inverter 1 and inverter 2. For example, the voltage of inverter 1 is set to be constant 100 V, and inverter 2 will be reduced in variations, such as 50 V and 70 V. The performance of the new sector definitions will be evaluated and analyzed based on their ability to reduce the percentage of THD, improve the quality of stator current, minimize the stator flux droop condition, and enhance torque performance for each speed conditions. Section 2 of this paper will give a brief idea of the basic DTC operation using an open-ended system. Section 3 will discuss the problem faced by the dual-inverter technique during an imbalance battery voltage supply. Subsequently, in Section 4, the discussion will be based on the conventional sector for balanced supply voltage and the proposed method using different sector definitions for different supply voltage. The experimental results will be analyzed in Section 5 under two categories namely steady state operation and transient speed condition. For steady state operation, three types of voltage ratios are tested within three speed condition. During transient state operation, the speed of a system is changes dynamically as to observe its performance and behaviour. Finally, the conclusion for this paper is in Section 6.

2. Dual inverter DTC-OEWIM

The following space vector equations, stated in the stator stationary reference frame, are used to express the dynamic modeling of an induction machine in DTC drives:

$$\bar{v}_s = R_s \bar{i}_s + \frac{d\bar{\varphi}_s}{dt} \tag{1}$$

$$0 = R_r \bar{i}_r - j\omega_r \bar{\varphi}_r + \frac{d\bar{\varphi}_r}{dt} \tag{2}$$

$$\bar{\varphi}_s = L_s \bar{i}_s + L_m \bar{i}_r \tag{3}$$

$$\bar{\varphi}_r = L_r \bar{i}_r + L_m \bar{i}_s \tag{4}$$

$$T_e = \frac{3}{2} P \bar{\varphi}_s \times \bar{i}_s = \frac{3}{2} (\bar{\varphi}_{sd} i_{sq} - \bar{\varphi}_{sq} i_{sd}) \tag{5}$$

where $\bar{v}_s$ represents the stator voltage; $\bar{\varphi}_r$ and $\bar{\varphi}_s$ are rotor and stator flux, respectively; $\bar{i}_r$ and $\bar{i}_s$ are rotor and stator current, respectively; ω_r denotes the rotor angular speed in rad/s. Meanwhile, L_s, L_r, L_m, R_r, and R_s refer to the stator self-inductance, rotor self-inductance, mutual inductance, rotor resistance, and stator resistance, correspondingly. Here, T_e represents torque, and P stands for the number of poles pair. The dual-sided DTC shown in Fig. 1 comprises a set of subsystems consisting of a pair of hysteresis comparators to form a three-level hysteresis torque comparator and one unit of hysteresis to realize the two-level hysteresis flux comparator. It also includes a switching information block in the look-up table, a stator flux estimator, a coupled 2-level voltage source inverter and a three-phase IM with an open-end winding configuration. Fig. 2 demonstrates the configuration of the dual-inverter circuit, which connects the two inverters through the winding of the IM. It comprises 12 units of power switches and separated voltage supplies to avoid the most known problems, namely common mode currents.

Fig. 3(a) and 3(b) illustrate the space vector structure of inverter 1 and inverter 2, respectively, with their switching states. The vectors are marked with '+' and '-', which indicates the status turned ON or turned OFF status for the upper switch of the inverter leg. For example, a voltage vector of V4 with 011 switching states indicates the phase-A leg either (S_a^{1+} or S_a^{2+}) is in OFF state and phase-B (S_b^{1+} or S_b^{2+}) and phase-C (S_c^{1+} or S_c^{2+}) is in turned ON state. As the topology of the circuit is added with a NOT gate at the lower leg, the switching information for the lower leg will be inverted or vice versa from the default switching information.

To realize the voltage vectors location shown in Fig. 3(c), the phase voltage across the stator winding of the dual inverter supplied drive can be formulated as follows:

$$v_{AA'} - v_{A'N'} - v_{NN'} \tag{6}$$

$$v_{BB'} = v_{BN} - v_{B'N'} - v_{NN'} \tag{7}$$

$$v_{CC'} = v_{CN} - v_{C'N'} - v_{NN'} \tag{8}$$

where the v_{XN} and $v_{X'N'}$ are the poles' voltage measured at every inverter leg, $v_{XX'}$ is the phase voltage, and X indicates phases A, B, and C. Hence, the different voltage between two negative rails of Direct Current (DC) supplies, also known as common mode voltage, $v_{NN'}$ can be written as

$$v_{NN'} = \frac{1}{3}[(v_{AN} - v_{A'N'}) + (v_{BN} - v_{B'N'}) + (v_{CN} - v_{C'N'})] \tag{9}$$

Substitute (9) into equations (6)-(8) to form the matrix form as follows:

$$\begin{bmatrix} v_{AA'} \\ v_{BB'} \\ v_{CC'} \end{bmatrix} = \frac{1}{3} \begin{bmatrix} 2 & -1 & -1 \\ -1 & 2 & -1 \\ -1 & -1 & 2 \end{bmatrix} \begin{bmatrix} v_{dc}(S_a^{1+} + S_a^{2+}) \\ v_{dc}(S_b^{1+} + S_b^{2+}) \\ v_{dc}(S_c^{1+} + S_c^{2+}) \end{bmatrix} \tag{10}$$

From (10), a total of 64 voltage vectors can be generated and classified into three different categories, namely short voltage vectors ($\bar{v}_{sS,1} - \bar{v}_{sS,6}$), medium voltage vectors ($\bar{v}_{sM,1} - \bar{v}_{sM,6}$), and long voltage vectors ($\bar{v}_{sL,1} - \bar{v}_{sL,6}$), which are mapped in d_s and q_s axis.

3. Mismatch supply DC link voltage

3.1. Problem formulation

In the dual-inverter technique, the power packs are connected individually at both ends of the induction motor through a power inverter circuit. For EV applications, suitable power packs such as batteries or supercapacitors can provide instantaneous current demand during dynamic operation [31–33]. However, the DTC strategies for dual-inverters use the default switching table suitable for fixed DC-link voltage. This dual-inverter technique can change its behavior from the default symmetrical to asymmetrical types when the inverter is fed with different voltage levels. Based on [34,35], the asymmetrical studies are mainly focused on increasing the voltage inversion by modifying the hysteresis band controller.

Therefore, this manuscript will discuss a problem faced by the dual-inverter technique due to the mismatch of two isolated DC supplies. During the study, it is noticeable that the

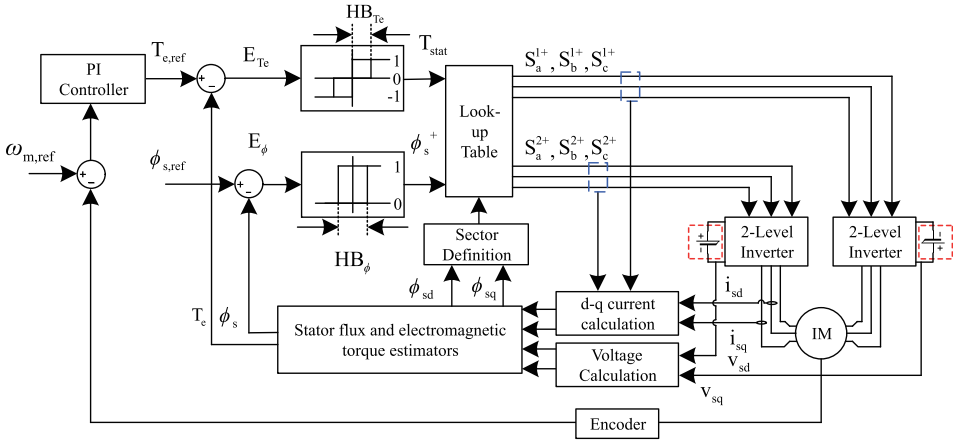

Fig. 1 The dual-inverter technique for Open-End Winding DTC System.

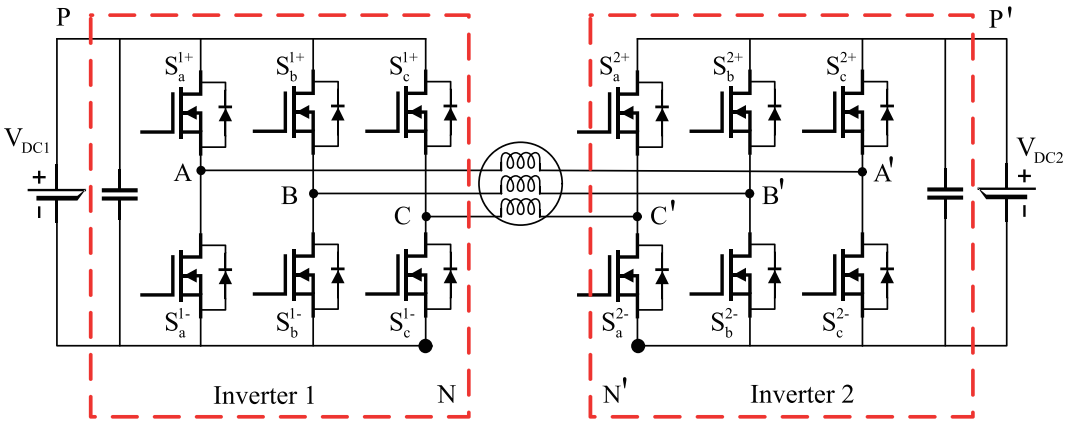

Fig. 2 The configuration of dual-inverter technique.

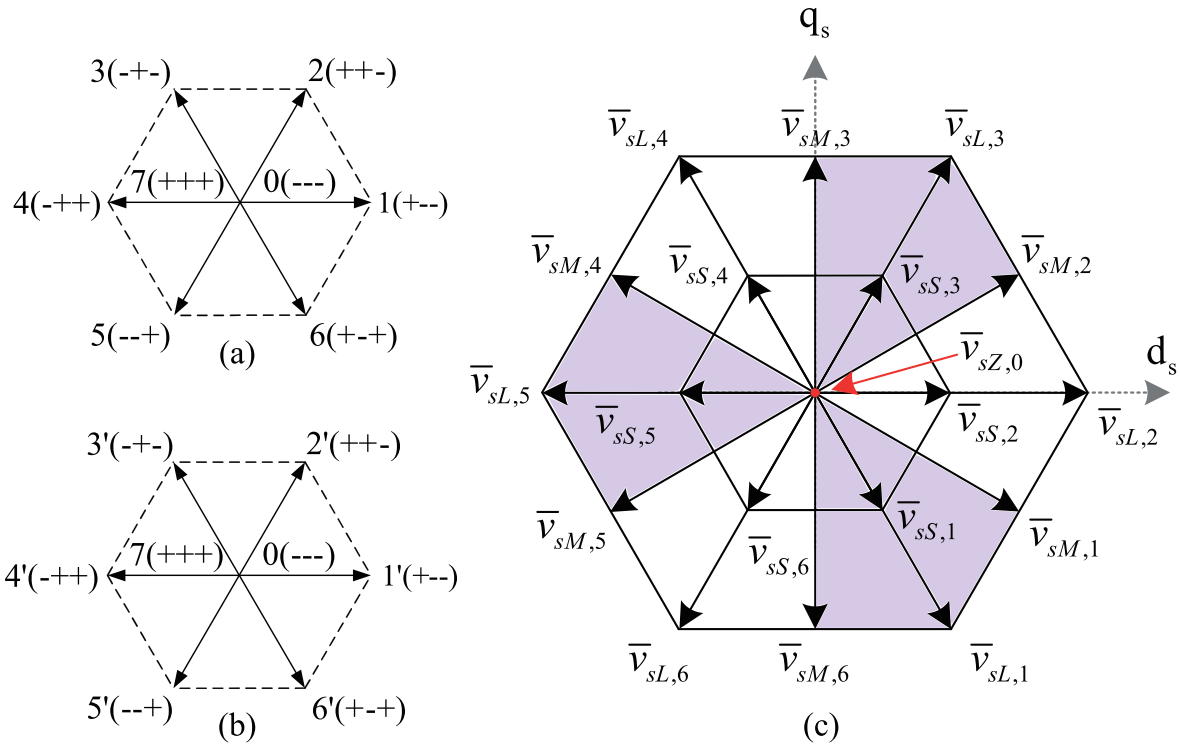

Fig. 3 The dual inverter switching states and mapping.

angle of the resultant vector between two inverters is tilted irregularly during the mismatch of the voltages, especially when DTC chooses a medium voltage vector, as depicted in Fig. 4. Other than that, the voltage vectors for short and long vectors were also affected in term of reduction in magnitude. Still, the condition of the angle is maintained as the matched DC voltage.

The tilted voltage vector in the medium vectors will affect the movement of stator flux in the default sector definitions, where it is equally divided by a 60° angle. As a result, the distorted voltage vectors will no longer be tangential to the default flux vector. To address the resultant voltage vector, the stator voltage of the inverter (11) is defined in a stator stationary reference frame, which includes $d-$ and $q-$ axis coordinates. Hence, it is rewritten into rectangular form by considering Euler's Theorem and separating it into real and imaginary sections as (12) and (13).

$$\bar{v}_s = \frac{2}{3}(v_{AA'} + \bar{a}\, v_{BB'} + \bar{a}^2 v_{CC'}) \tag{11}$$

$$\begin{aligned}\bar{v}_{sd^s} &= \mathrm{Re}[\frac{2}{3}(v_{AA'} + \bar{a}\, v_{BB'} + \bar{a}^2 v_{CC'})] \\ &= \frac{1}{3}(2v_{AA'} - v_{BB'} - v_{CC'})\end{aligned} \tag{12}$$

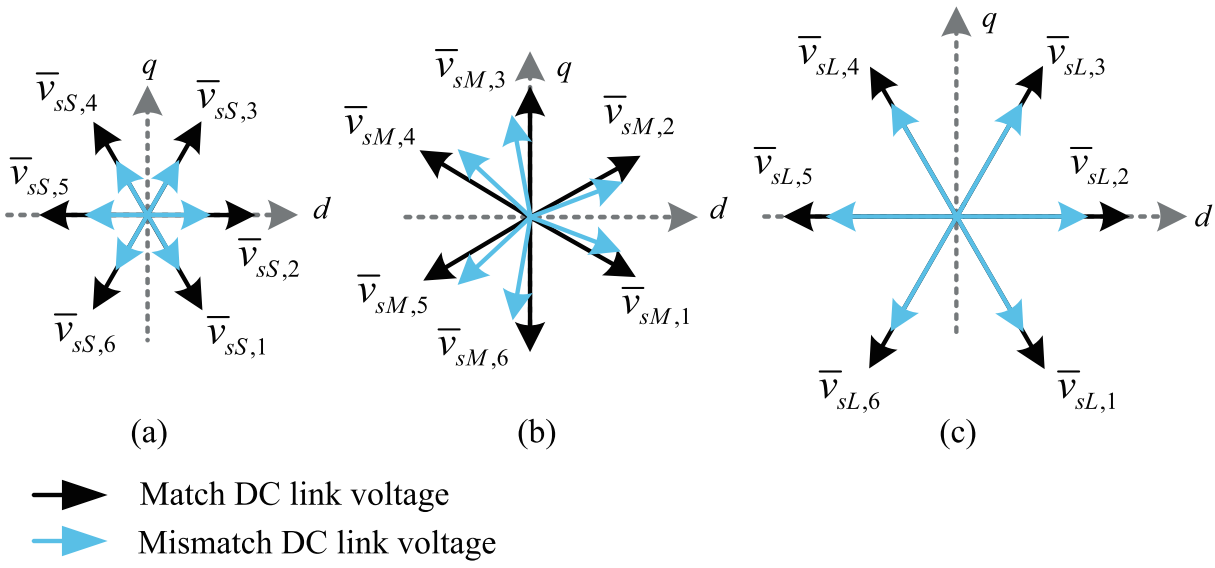

Fig. 4 Different between match and mismatch DC link voltage in (a) Short vectors (b) Medium vectors and (c) Long vectors.

$$\bar{v}_{sq^s} = \mathrm{Im}[\frac{2}{3}(v_{AA'} + \bar{a}\, v_{BB'} + \bar{a}^2 v_{CC'})] = \frac{1}{\sqrt{3}}(v_{BB'} - v_{CC'}) \tag{13}$$

Equation (11) can be substituted into (12) and (13) to produce the stator voltage components in terms of switching states as follows:

$$\bar{v}_{sd^s} = \frac{V_{dc}}{3}\left[2\left(s_a^{1+} - s_a^{2+}\right) - \left(s_b^{1+} - s_b^{2+}\right) - \left(s_c^{1+} - s_c^{2+}\right)\right] \tag{14}$$

$$\bar{v}_{sq^s} = \frac{V_{dc}}{\sqrt{3}}\left[\left(s_b^{1+} - s_b^{2+}\right) - \left(s_c^{1+} - s_c^{2+}\right)\right] \tag{15}$$

And the magnitude,$|\vec{a}|$ of resultant voltage vector:

$$|\vec{a}| = \sqrt{\left(v_{sd^s}\right)^2 + \left(v_{sq^s}\right)^2} \tag{16}$$

3.2. Effect on resultant voltage vector

The process of generating the resultant voltage vectors is illustrated in Fig. 5(a) and (b) for match and mismatch voltage, respectively. During the balanced DC link voltage, both inverters are fed equally with 100 *V*. To trigger the power switches, the binary number system shown in Fig. 3(a) and (b) indicates the switching state according to predefined sector definitions. For example, in the match DC-link voltage, the switching states of (100001) will trigger the (100) at inverter 1 and (001) to inverter 2 to generate the resultant voltage vector of $\bar{v}_{sM,2}$. The resultant vector through a combination of $\bar{v}_{sd^s}$ = 100 *V*, $\bar{v}_{sq^s}$ = 57.74 *V* generates a phase angle approximately 30° from the origin V_d plane in the Fig. 5(a). Consequently, when the switching states of (100001) are applied to the mismatch DC link voltage (inverter 1 = 100 *V*, inverter 2 = 50 *V*), the generation of $\bar{v}_{sd^s}$ and $\bar{v}_{sq^s}$ are affected and resulting the phase angle of resultant voltage vectors is reduced from 30° to 19.11°.

4. The proposed new sector definitions

4.1. Formulating new sector definitions

In the default system with a stable DC link supply, the profile of the current waveform is excellent due to the selection of the voltage vector being more tangential for every sector as shown in Fig. 6a. This is the example of voltage ratio 100:100. However, as explained in Section 3, the voltage vectors in the mismatch DC link voltage are tilted, and the rate of tilted will be greater if there is a larger difference between supply voltage. This will result in the position of the voltage vectors being less tangential to the flux vector in the conventional sector definitions, as in Fig. 6b. Apart from that, this condition will result in poor vector movement in terms of angular frequency in the circular loop, resulting in the bad performance for the whole system.

Thus, a new sector definition is designed by ensuring the plotted sector borderline is 90° from the most tangential voltage vector, as illustrated in Fig. 7(a). Three examples were given where borderline for $\bar{v}_{sM,1}$, $\bar{v}_{sM,3}$, and $\bar{v}_{sM,5}$ is placed exactly at a 90° angle. The complete six sector definitions are displayed in Fig. 7(b). This is the example for sector definitions with a ratio of (inverter 1 = 100 *V*, inverter 2 = 50 *V*). Based on studies, the angle of 90° degrees should be placed in the correct position to allow the voltage vector movement to be more tangential to the flux vectors. Since the battery in EV drain varies with time and depends on the load, the pre-defined angle is prepared to cater the possible of a new voltage ratio and the selection is made through voltage sensing and selection of the sector definitions. However, not every voltage drop need to be calculated and need a new sector definition. From the study, approximately for every 5 V voltage difference need a new sector as the angle difference is far and might affecting the generation of stator currents, thus affects the performance of torque and stator flux as well. If lesser than that, the movement of voltage vectors are still in range and not effecting the performance much.

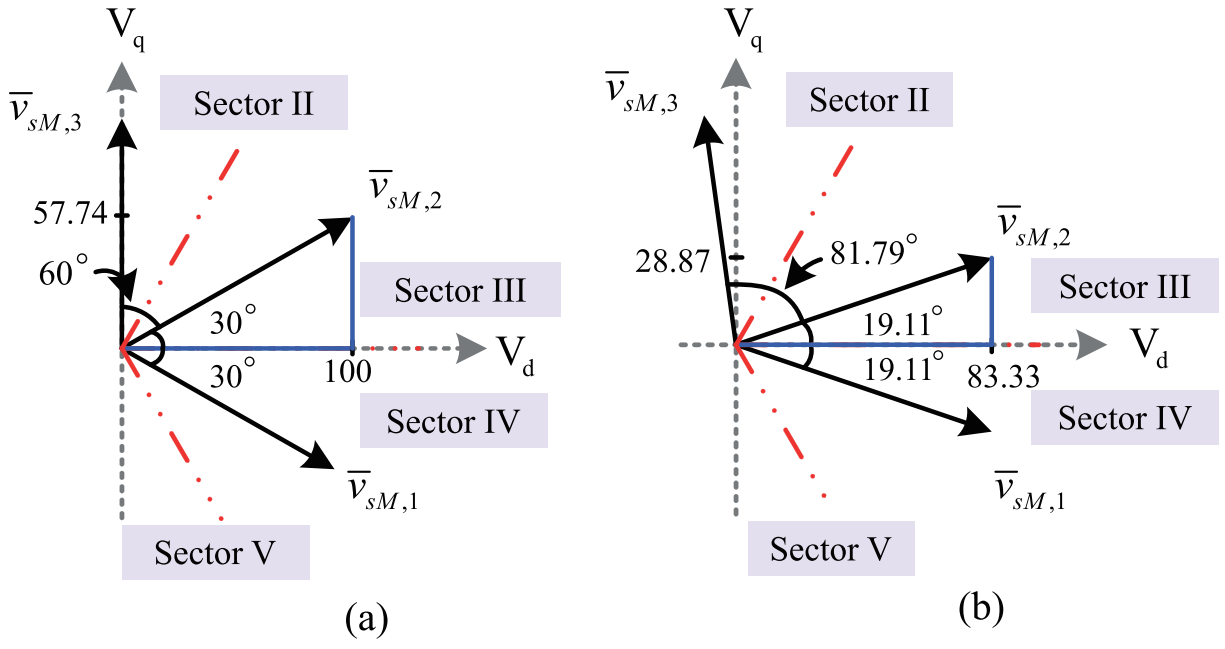

Fig. 5 Generation of resultant voltage vectors (a) match DC-link voltage (b) mismatch DC-link voltage.

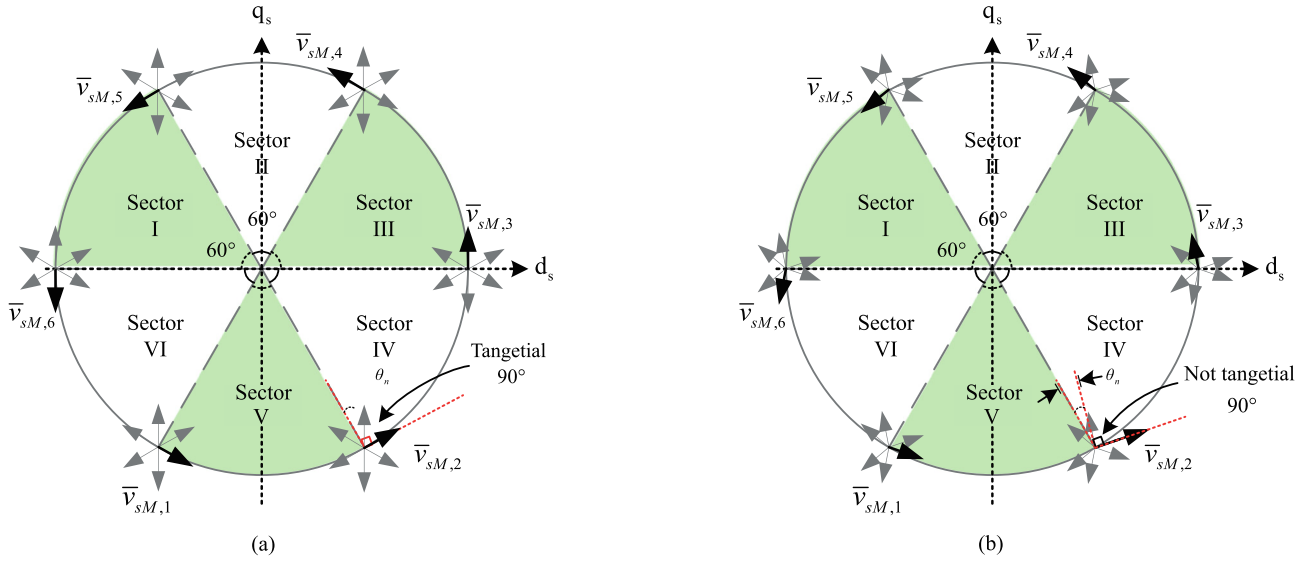

Fig. 6 Mapping of voltage vectors in default sector definitions (a) Match DC voltage (standard voltage vectors) (b) Mismatch DC voltage (tilted voltage vectors).

To easily design the new sector definitions for each voltage conditions, angle sector, θS_n can be formulated:

$$\theta S_n = \left(\tan^{-1}\left(\frac{v^s_{sq,n}}{v^s_{sd,n}}\right)\left(\frac{180}{\rho}\right)\right) - 90^{\circ} \tag{17}$$

Where $v_{sqd^s,n}$ and $v_{sq^s,n}$ is the generated D-Q voltage from equation (14) and (15) whenever there is a change in the DC-link voltage at inverter 1 and inverter 2. The calculated angle then needs to be mapped in the 4 quadrat of sectors and considering the conditions of tangent value for each quadrant. This pre-calculated algorithm is embedded in the system by replacing the conventional sector detection with the modified sector detection block as shown in Fig. 8. The flow to calculate the angle for each sector portrays in Fig. 9.

4.2. Implementing new sector definitions

Fig. 10(a) and Fig. 10(b) portrays the new sector definitions for an inverter ratio of 100:50 and 100:70 respectively. As observed, the voltage vectors can now be placed appropriately and tangential to the flux sector condition. This will retune the movement of the voltage vector and allow the flux to be controlled in a circular locus again and rarely cross the hysteresis band limit. Note that the new sector no longer has an equal

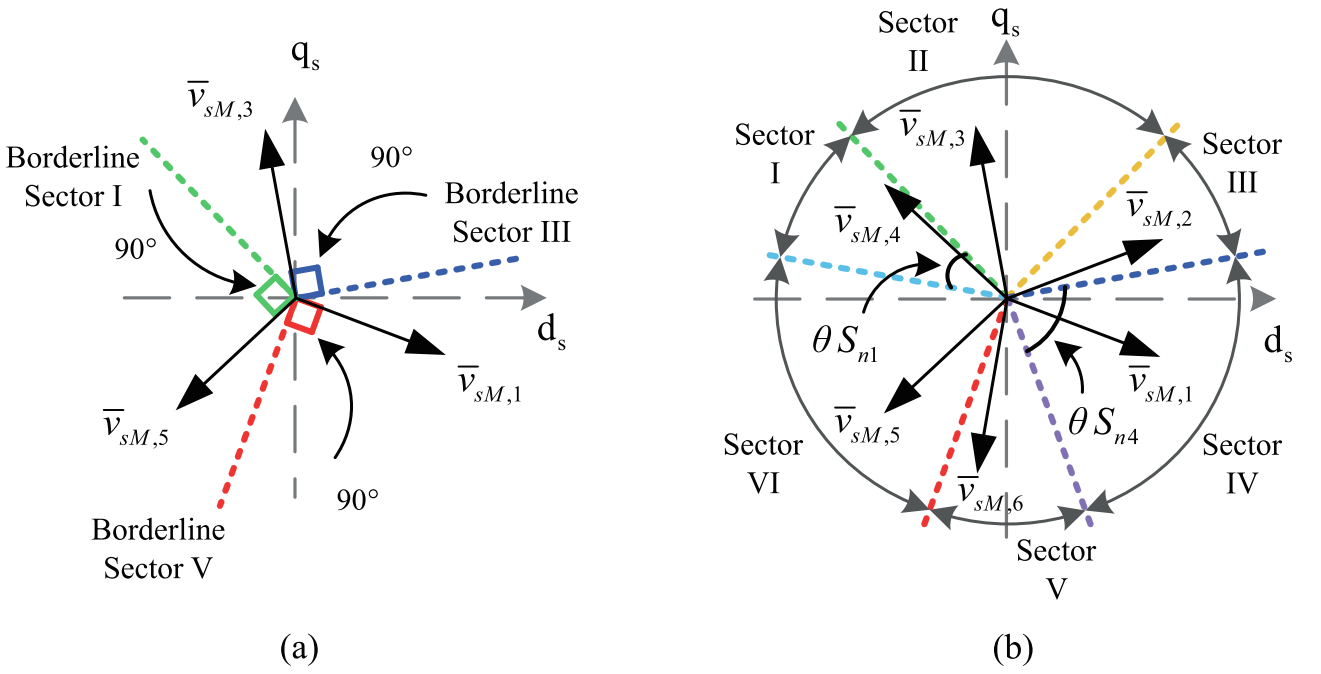

Fig. 7 Remapping the new sector definitions for inverter ratio 100:50. (a) Partially for 3 voltage vectors (b) Complete 6 voltage vector.

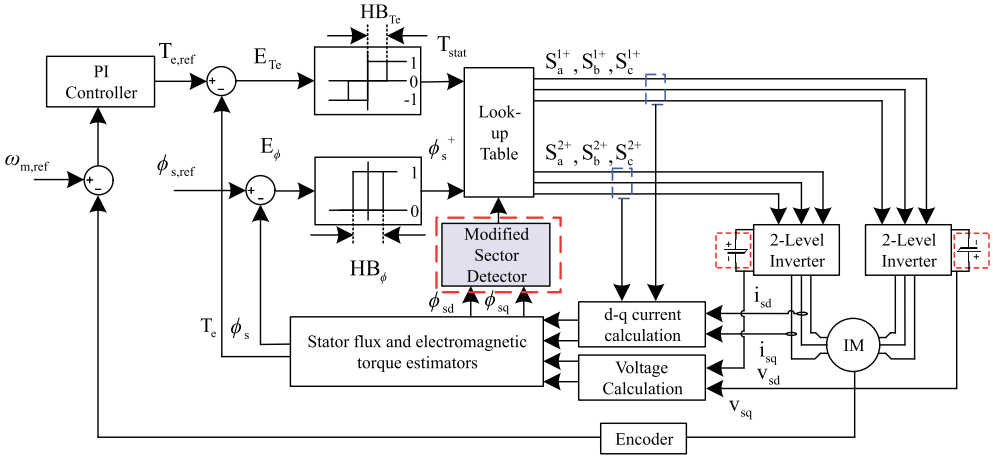

Fig. 8 Mapping of affected voltage vectors to the default sector definition.

phase angle for each sector. It will change according to the level of voltage injected into both inverters. Using the same voltage vector at the newly proposed sector definitions, the voltage vector can be placed appropriately and tangentially to the flux sector condition. This will retune back the movement of the voltage vector and allows the flux to be controlled in a circular locus again. As mentioned earlier, this study is tested for two different conditions of voltage ratio, namely 100:50 (inverter 1:100 *V*, inverter 2: 50 *V*) and 100:70 (inverter 1:100 *V*, inverter 2: 70 *V*). This pre-calculated algorithm is embedded in the system by replacing the conventional sector detection with the modified sector detection block diagram. The speed ω_s of the motor will be controlled by adjusting the load at the induction motor.

5. Results and discussion

5.1. Experimental setup and Parameter

The problem of unstable voltage in EV applications was presented, especially in the experimental section. In practice, the EV will move on terrain such as straight roads, rocky roads, etc. The terrain that causes higher friction to the wheel will cause a larger power consumption, and sometimes the power absorption is not stable between the inverters. To address these issues, experimental testing has been conducted by driving the three-phase induction machine with the parameters tabulated in Table 1. To realize the DTC-OEWIM system for this EV study, a lab-scale experimental setup consists of a squirrel cage

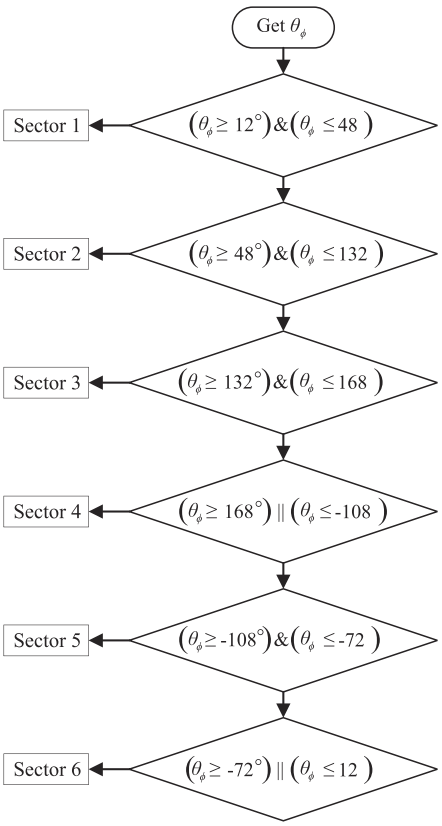

Fig. 9 Flowchart to calculate the angle for each sector.

IM with 1.1 kW power rated with a rated speed of 2800 rpm is connected to a separated DC supply using a dual inverter technique as shown in Fig. 11. Note that each inverter is powered up with 100 *V* supply, resulting in the full system is feed with 200 *V* supply voltage. The control algorithm of DTC is performed using the dSPACE 1104 controller board, and the selected sampling time is 50 μs. The experimental results are captured through the digital oscilloscope Tektronix DPO 3034 Digital Phosphor.

The feasibility of the proposed sector definitions is validated through the experimental assessment, and it is conducted in two different voltage ratios with a constant torque reference of 1.5 N_m. Each was tested with three different speed operations, low-speed (300 rpm), medium-speed (600 rpm), and high-speed (1000 rpm). Other than that, the experimental results are presented and analyzed in detail, including the stator current behavior, torque performance, and THD. The performance of results demonstrated, such as stator currents, I_a, I_b, I_c, torque, T_e, speed, ω_s, and the harmonic current, THD_i.

5.2. Experimental results

A. Steady state operation.

A match DC voltage between two invertes will form a VD-VQ voltage with an equal 60° angle per sector as in Fig. 12(a). While in mismatch case, the inverter will generate a tilted voltage, as depicted in Fig. 12(b) and Fig. 12(c) for inverter ratios of 100:50 and 100:70, respectively. The following results compare conventional and proposed techniques in the same windows initiated by triggering the flag signal. The following Fig. 13, Fig. 14, and Fig. 15 depict the results obtained for three different inverter ratios, namely 100:100, 100:50, and 100:70 respectively. Each of the results portrays the same arrangement as follows; first trace: torque (Nm), second trace: stator flux (Wb), third trace: stator currents (A), fourth trace: VD (V), fifth trace: VQ (V), sixth trace: speed (rpm).

To make a significant comparison between matched and mismatched voltage conditions, a default condition using a stable DC link voltage is necessary to observe the default conditions of each waveform. Fig. 13(a), Fig. 13(b), and Fig. 13(c) depict the results obtained for an inverter ratio of 100:100 at high, medium, and low speeds, respectively. During stable voltage injection, the voltage vectors move uniformly in a direction that generates stator currents in normal conditions for each speed condition. As the motor enters the low speed zone, the torque begins to show significant ripple conditions. Despite high ripples, the torque still moves in a uniform zigzag pattern, as shown in the magnified version. This criterion is important to achieve constant switching conditions. Next,

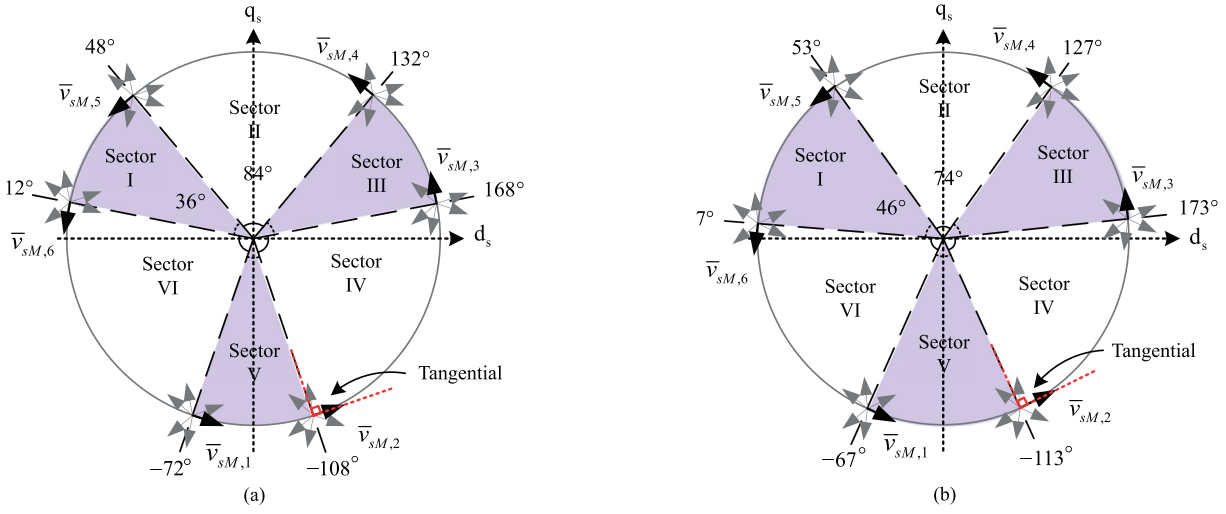

Fig. 10 New sector definitions for voltage ratio of (a) 100:50 (b) 100:70.

Table 1 The induction machine parameters.

Induction Machine	
Parameter	Value
Stator Resistance,R_s	6.1 Ω
Rotor Resistance,R_r	6.2293 Ω
Mutual Inductance,L_m	0.4634 mH
Rotor self inductance,L_r	0.47979 mH
Stator self inductance,L_s	0.47979 mH
Number of pole pairs, P	2
Conventional and Alternate Switching of DTC system	
Torque Hysteresis band,HB_{Te}	0.5 Nm
Flux Hysteresis band,HB_{φ}	0.0080 Wb

the stator flux (second trace) begins to form a large droop phenomenon during low-speed operation. One reason is that the stator resistance has a larger effect on the stator voltage at low speeds. At low speeds, the back electromotive force (EMF) of the motor is also smaller, which means that the stator voltage must be larger to maintain a constant flux level. However, since the stator resistance has a larger effect on the voltage drop at low speeds, the effective voltage applied to the motor is reduced, leading to stator flux droop. The VD and VQ generations are stable and do not face any distortion. The last trace is the rpm for each speed condition between high speed (1000 rpm), medium speed (600 rpm) and low speed (300 rpm).

In the following results for inverter ratio 100:50 and 100:70, the results are compare between conventional and proposed sector definitions in the same windows initiated by triggering the flag signal. Fig. 14 illustrates the inverter response after varying voltage ratios under 100:50 conditions. The condition of stator currents faced a distortion and appears to have a large notching effect when operating the inverter using the default stator definitions. When there is a significant difference in voltage ratio, the voltage vectors may become tilted, as illustrated in Fig. 4, particularly when using medium voltage vectors. If the selected voltage vector is not aligned with the estimated stator flux vector, it can result in a large difference between the reference and actual stator current, leading to notching in the current waveform. Notice that the distortion repeatedly occurs at the same location for every cycle. This is where the flux changes its direction between the positive side locus and the negative side locus. Usually, the positive side locus will be in the region of sector k + 1, and the negative side locus will be in the region of sector k-1. The torque performance in the default sector also poor and not well regulated. It seems to have a distortion in the same interval and most likely following the stator current performance. The torque behaviour not uniform in a zig-zag pattern and also decrease sharply as shown in Fig. 14(a) and Fig. 14(b) respectively. The performance of stator flux also suffers from large droop during the conventional technique simultaneously for 3 speed cases. The results of VD and VQ is the same for both conventional and proposed sector as the generation of VD and VQ is based on inverter switching state and inverter voltage and not affecting by the proposed sector. The distortion in VD and VQ voltage is due different voltage ratio injection to the inverter.

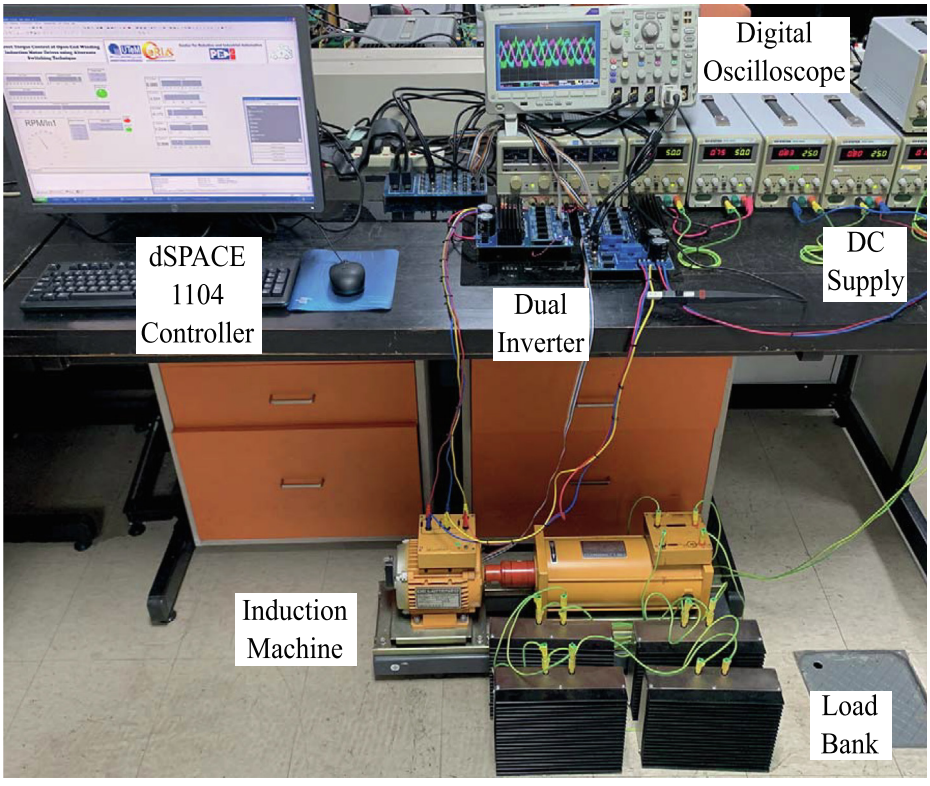

Fig. 11 Lab scale experimental setup.

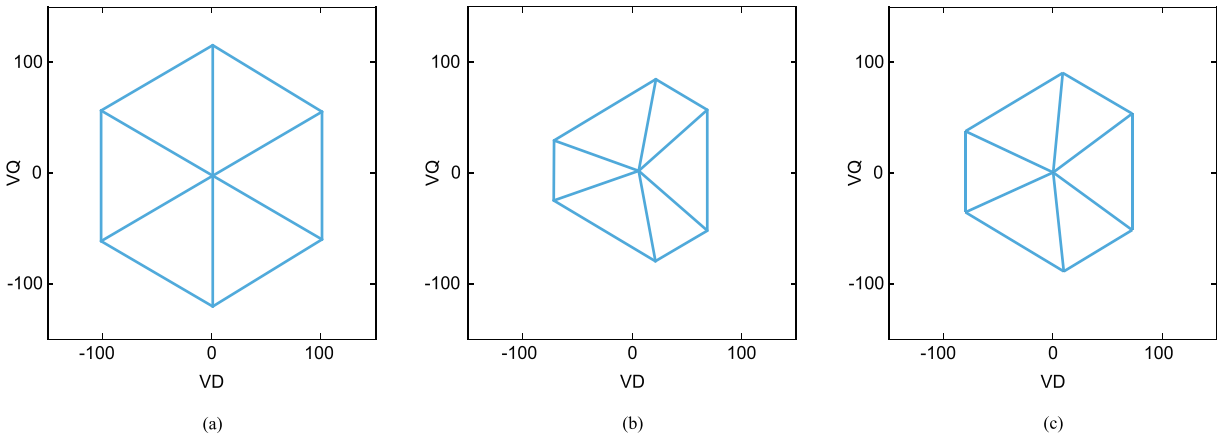

Fig. 12 VD-VQ locus for each Inverter ratio (a) 100:100 (b) 100:50 and 100:70.

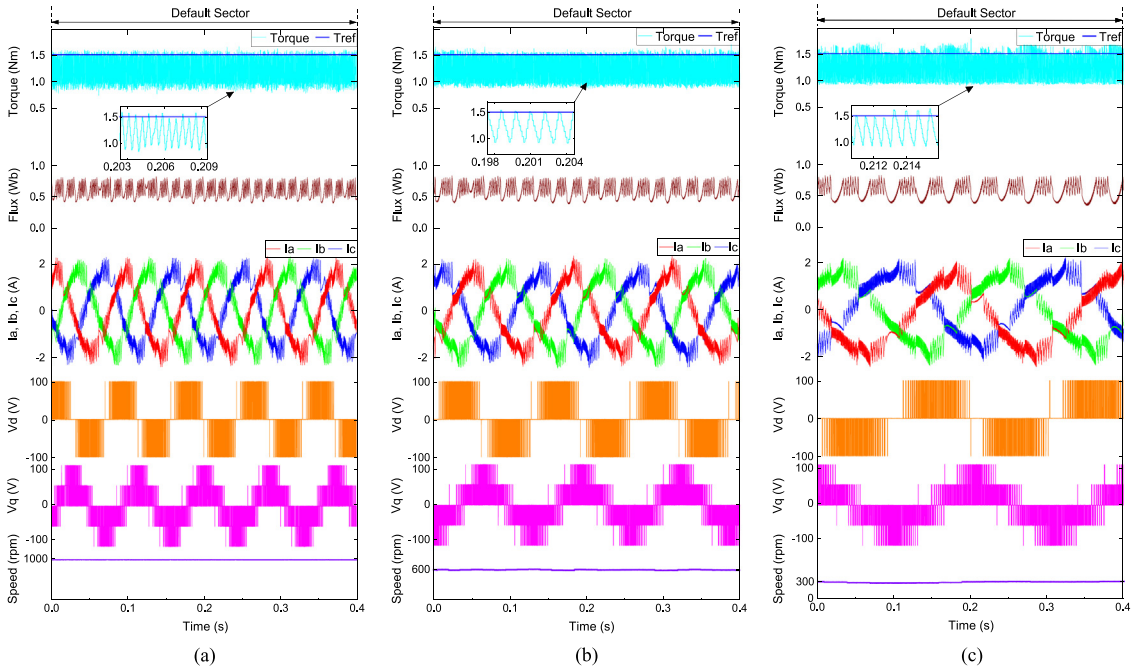

Fig. 13 Performance of torque, stator flux, stator currents, VD, VQ and speed on conventional and proposed sector definitions under Inverter ratio of 100:100 for (a) High Speed (b) Medium Speed (c) Low Speed.

However, when the proposed sector for 100:50 is triggered, the regular interval of the notching effect in the stator current starts to reduce the spike and curve, as shown in Fig. 14(a) in the dotted black box. This situation is the same for medium speed and low-speed conditions. The performance of torque in the proposed sector also starts to improve and regulate in a uniform zig-zag pattern, and the selection of reverse voltage vectors no longer occurs as there is no sudden torque decrease phenomenon. The stator flux droop improves significantly, reducing to almost 0.3 Wb with the proposed sector definition. This criterion is important because a large droop can cause poor torque control, and variations in the stator flux magnitude and angle can lead to an increase in the current harmonics generated by the motor.

Correspondingly, the assessment also tested an inverter ratio of 100:70, shown in Fig. 15 in the same three speed condition as in Fig. 15(a), Fig. 15(b) and Fig. 15(c). On the ratio of 100:70, the stator currents still suffers from the interval notching effect and the torque regulation still in poor condition during the conventional sector definitions. However, the distortion effect is not intangible as in the ratio of 100:50. The condition of stator flux droop also poor, but it is not critical as inverter ratio of 100:50. Fortunately, when the proposed sector is enabled, the flag is initiated, the distortion at the stator currents starts to reduce its magnitude, and the notching curve becomes smaller for both the positive and negative sides. The improvement using proposed sector definitions applies for all speed ranges. The performance of torque improves in the proposed sector as the movement of torque more uniform and not crossing the torque reference limit. While for stator flux droop performance also improves and reduceds the droop size up to 0.2 Wb. The waveform of the VD and VQ voltages

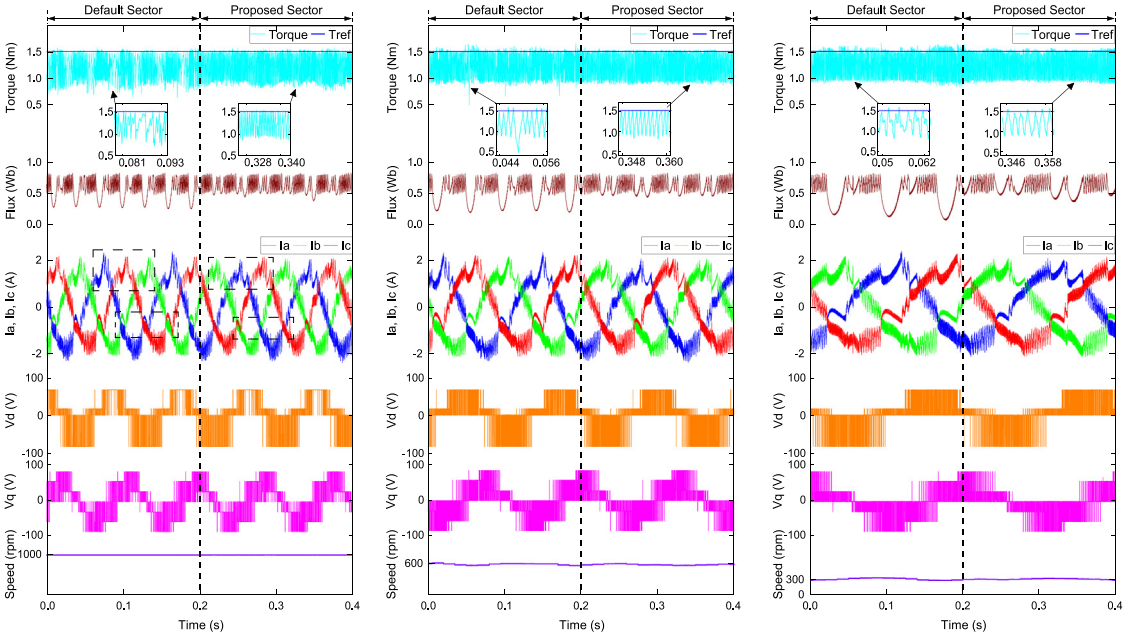

Fig. 14 Performance of torque, stator flux, stator currents, VD, VQ and speed on conventional and proposed sector definitions under Inverter ratio of 100:50 for (a) High Speed (b) Medium Speed (c) Low Speed.

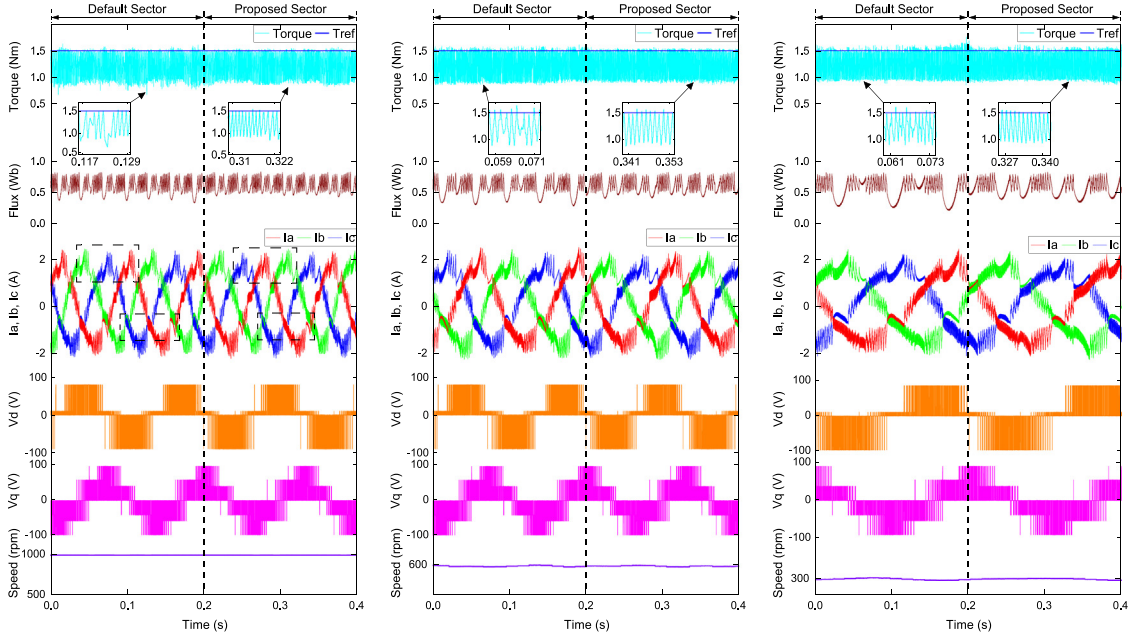

Fig. 15 Performance of torque, stator flux, stator currents, VD, VQ and speed on conventional and proposed sector definitions under Inverter ratio of 100:70 for (a) High Speed (b) Medium Speed (c) Low Speed.

for the 100:70 ratio is not as critical as for the 100:50 ratio, as it still appears fine, given that the voltage range between the two inverters is still close.

Figs. 16, 17, and 18 show the percentage of harmonic content in the low-order harmonic results for each inverter ratio, categorized into three different speed operations. Generally, the stator currents in the induction motor follow the triplen harmonic principle, where the odd integral multiples of the third harmonic, such as the 3rd, 9th, and 15th harmonics, either do not generate significant harmonics or generate harmonics that are too minor to be of importance. This is because the triplen harmonics are canceled out by the magnetic fields generated by the stator and rotor. Sometimes, the harmonic cancelation may not be perfect due to the non-linear of switch-

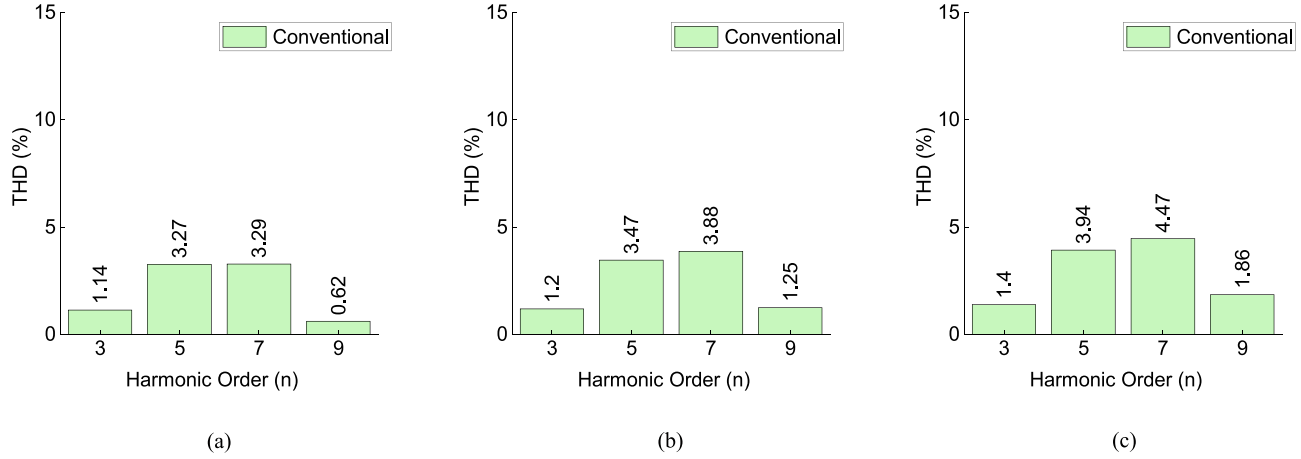

Fig.16 The percentage of low-order harmonic content for inverter ratio 100:100 ratio using conventional sector definitions (a) high speed (b) medium speed (c) low speed.

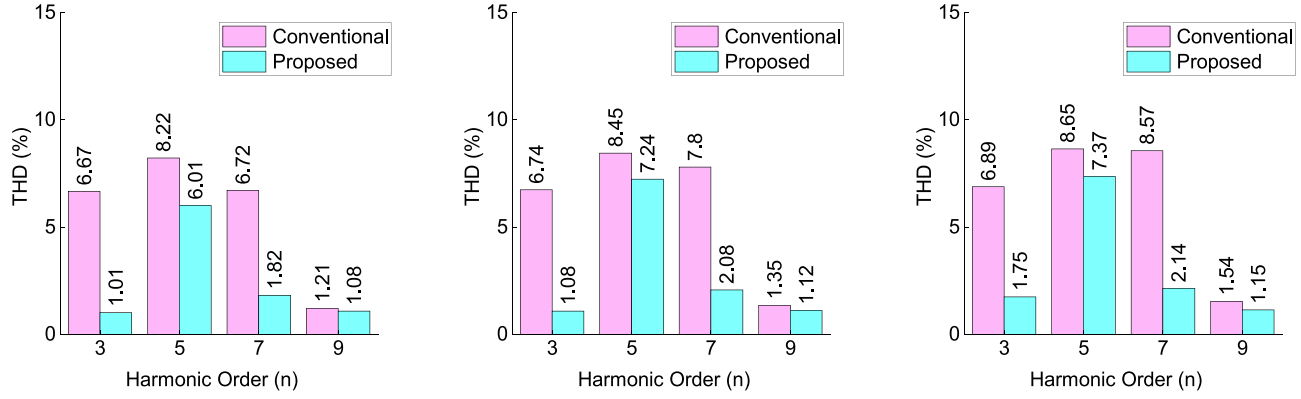

Fig.17 The percentage of low-order harmonic content for inverter ratio 100:50 ratio using conventional and proposed sector definitions (a) high speed (b) medium speed (c) low speed.

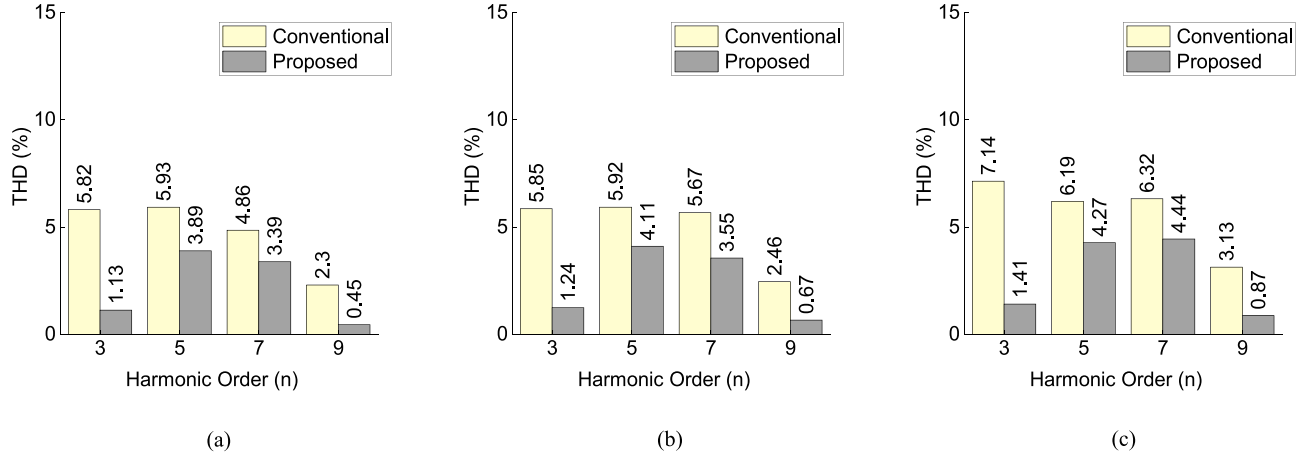

Fig.18 The percentage of low-order harmonic content for inverter ratio 100:70 ratio using conventional and proposed sector definitions (a) high speed (b) medium speed (c) low speed.

ing pattern especially in DTC system. Fig. 16 is a great example to show how the normal induction machine current behaviour as it is operates using 100:100 voltage ratio. The results indicate that the harmonic content at the 3rd and 9th orders is significantly lower than the harmonic at 5th and 7th orders. Additionally, the harmonic content gradually increases as the

speed of the induction motor is reduced. For instance, the percentage of the 7th harmonic order is 3.29% at high speed, but it increases to 4.47% when the speed of the induction motor is decreased.

Nevertheless, if the stator currents are distorted or not aligned in phase, they will not follows the triplen harmonic principle. This example can be observed at inverter ratio 100:50 and 100:70 at Fig. 17 and Fig. 18 respectively. In Fig. 17(a), the percentage of harmonic is approximately 6.67% in conventional sector, where naturally the reading should be low as this is categorized under triplen harmonic cancelation. Due to stator current waveform under this condition is distorted and has many notching effect, the reading of harmonic is interrupted. When the proposed sector is enabled, the percentage of harmonic at 3rd order drop to 1.01%, almost 5.66% reduction. For the harmonic order categorized under triplen harmonic such 3rd and 9th, the reduction of percentage between conventional and proposed sector are really significant as the waveform of stator current significantly improve and retune back to a normal stator current waveform. For non-triplen harmonic such 5th and 7th harmonic order, the percentage of harmonic reduction still occurs but not really significant as naturally the 5th and 7th harmonic order is high as it is not categorized as triplen harmonic cancellation. This similar scenario observeable in each harmonic order as illustrated in Fig. 17(a) – Fig. 17(c) and Fig. 18(a) – Fig. 18(c) at any speed condition for both 100:50 and 100:70 respectively.

The Total Harmonic Distortion (THD) percentage of the stator currents is excellent when the waveform closely resembles a sinusoidal pattern. However, in DTC-hysteresis based systems, the current waveform is not purely sinusoidal because the current randomly travels within predefined hysteresis upper or lower band limits to generate the inverter switching pattern. This continuous action results in a more zig-zag current pattern and not a sinusoidal one. A typical current in a DTC system that uses a hysteresis controller generates a current with a THD ranging from 15% to 18%, depending on the speed and waveform pattern, and sometimes it can go up to 30%. The complete reading of the THD currents for this study is tabulated in Table 2. Although the value of THD in the proposed sector is not less than 5%, it is accepted as this is the current that operates under an induction motor and uses a hysteresis-based controller. Based on Table 2, the inverter ratio 100:100 only has value for conventional section as it uses an equal voltage for inverter 1 and inverter 2 with default sector definitions. It is most likely that the reading of THD for 100:100 will be a major reference for the proposed sector of 100:50 and 100:70. As shown, the value of THD during high-speed operation is approximately 17.92% for the inverter ratio 100:100. Compared to the proposed sector of 100:50 and 100:70, the value is fairly close, where 18.65% and 18.87% are obtained, respectively. This means that the proposed sector is capable of improving the stator currents quite well as the THD values are nearly within the default THD range of induction machine current under DTC-hysteresis based. Similarly, for medium and low speed, the proposed sector helps in reducing the percentage of THD.

B. Transient state operation.

In a full EV system that is powered by a power pack such as batteries or supercapacitors, the pack will discharge quickly during acceleration mode. The transient state of an EV is categorized into low speed to high speed operation (acceleration) and high speed to low speed operation (deceleration). This study is important because during acceleration, the power pack, such as a supercapacitor, will provide a high power burst to accelerate the induction motor in an instantaneous movement.

The analysis for transient state is implemented for both inverter ratio 100:50 and 100:70 as to test the feasibility of the proposed sector definitions. As shown in Fig. 19(a) and Fig. 19(b), this is the results of inverter with ratio 100:50 performing the acceleration and deceleration using default sector definition. The range of speed changes is between 300 rpm and 1000 rpm during acceleration and vice versa during deceleration. It is noticeable that the performance of torque extremely suffers and not well regulated after change to high speed operation. The situation is vice versa during deceleration as the torque not properly regulated during high speed operation. When the proposed sector is enabled, the performance of torque during high speed significantly improved and regulated as in Fig. 20(a). Additionally, the torque performance during low speed in Fig. 20(b) has better torque regulation with less ringing or waving compared to the conventional sector shown in Fig. 19(b).

Meanwhile, the speed waveform (purple trace) exhibits some jerking effect during acceleration in the conventional sector, as indicated by the black arrow in Fig. 19(a). Fortunately, the acceleration of the motor become smooth when proposed sector is selected as shown in Fig. 20(a). The similar behaviour

Table 2 The THDi performance between conventional and proposed technique.

Speed Condition	Technique	THD%		
		Inverter Ratio		
		100:100	100:50	100:70
Low	Default	20.13	26.28	24.92
	Proposed	–	20.70	21.13
Medium	Default	18.58	25.92	23.17
	Proposed	–	19.29	19.83
High	Default	17.92	24.75	22.37
	Proposed	–	18.65	18.87

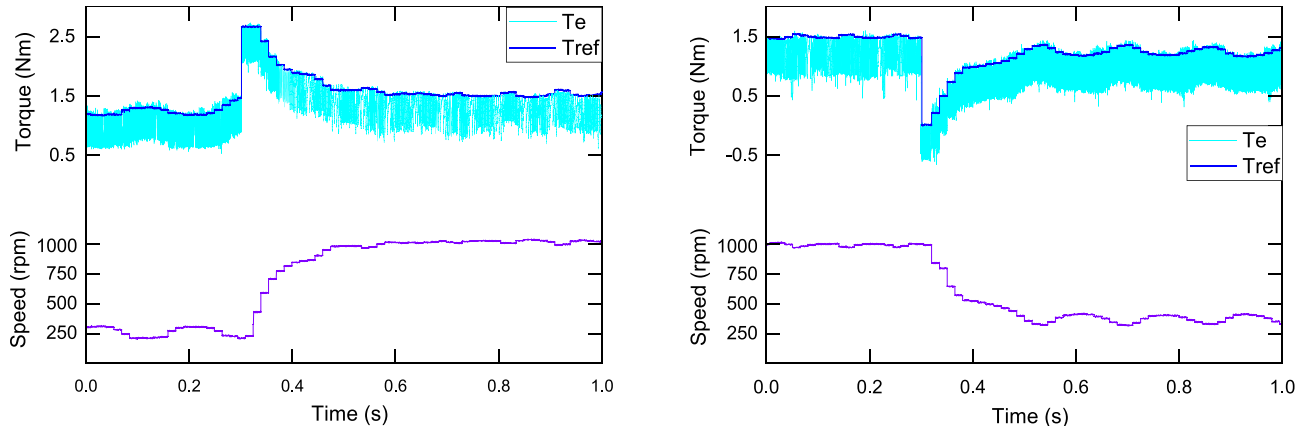

Fig.19 Transient operation using conventional sector for inverter ratio 100:50, (a) Low to high speed (b) High to low speed.

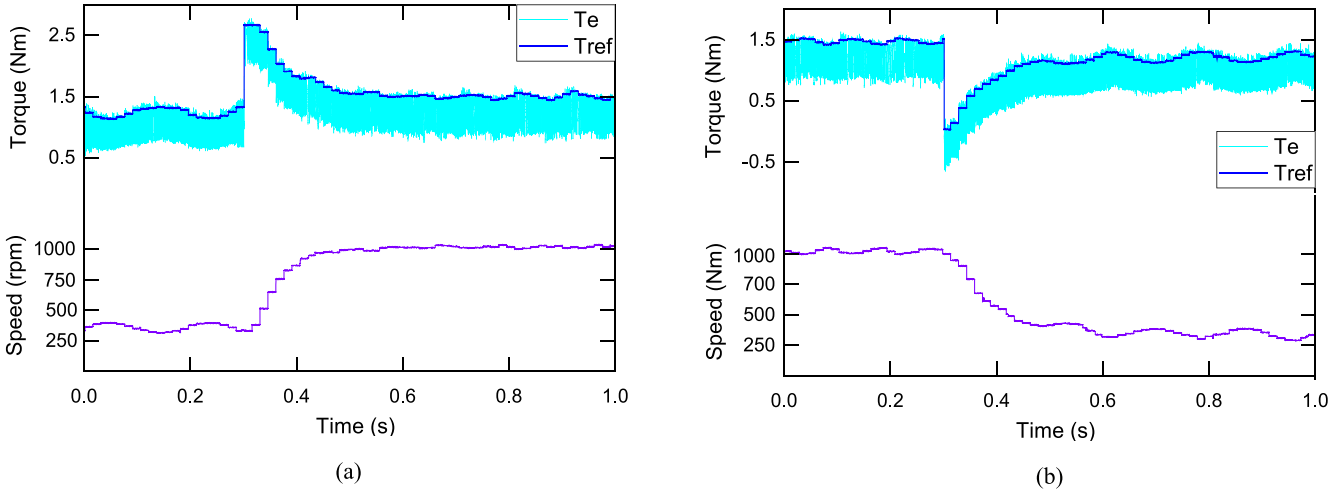

Fig. 20 Transient operation using proposed sector for inverter ratio 100:50, (a) Low to high speed (b) High to low speed.

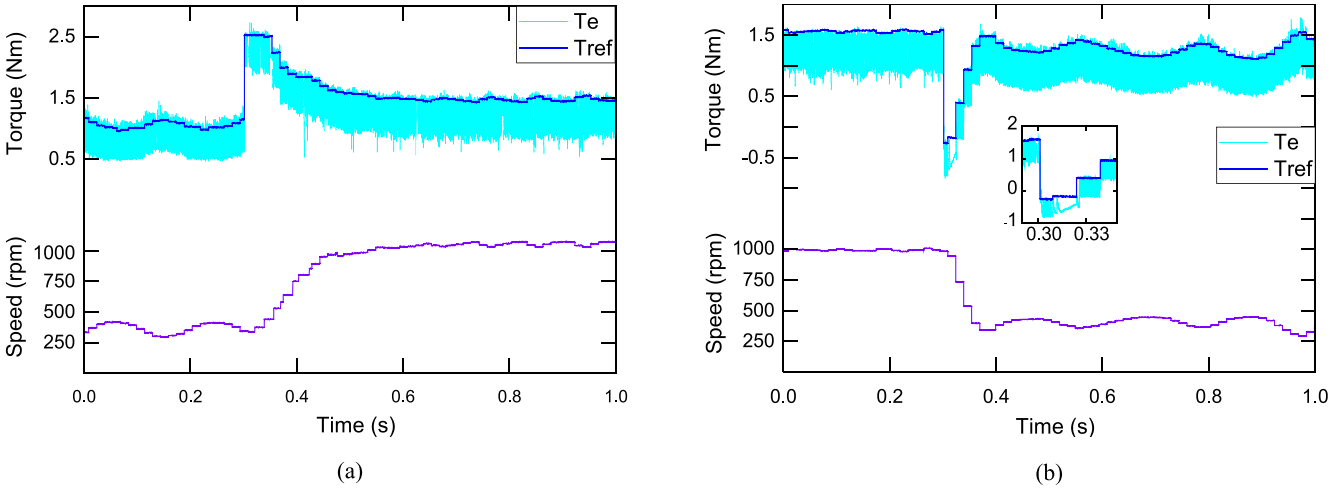

Fig.21 Transient operation using conventional for inverter ratio 100:70, (a) Low to high speed (b) High to low speed.

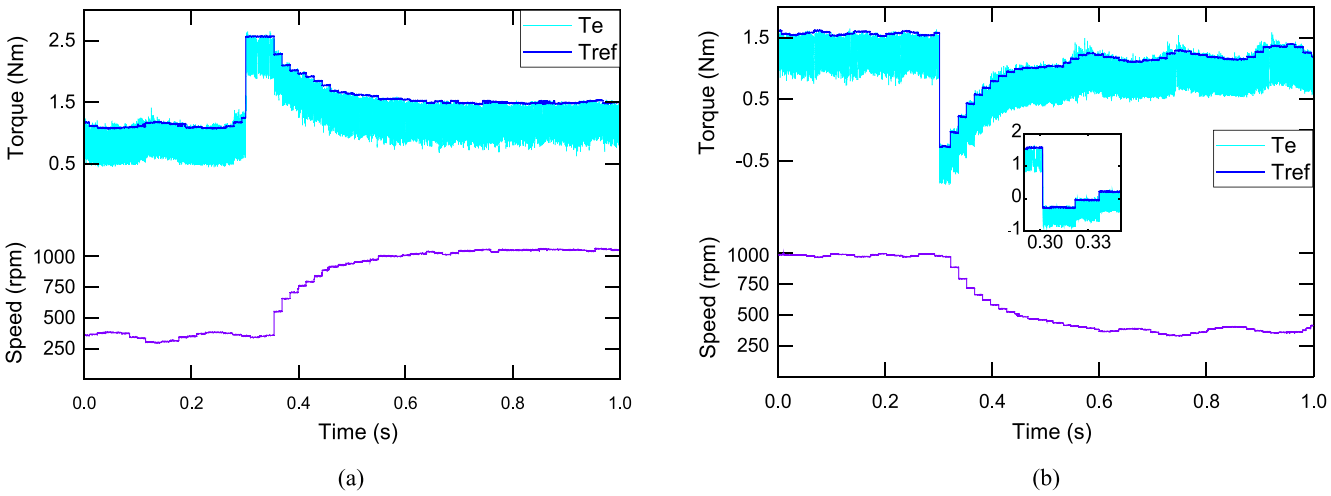

Fig.22 Transient operation using proposed for inverter ratio 100:70, (a) Low to high speed (b) High to low speed.

happened during deceleration process as portrays in Fig. 19(b) and Fig. 20(b).

The analysis continued for inverter ratio of 100:70, as demonstrated in Fig. 21 and Fig. 22. The behaviour is similar to previous study under 100:50 ratio. However in this study, the performance of torque fails to regulate during deceleration in Fig. 21(b). In the magnified version shows the torque seems to has a large inertia after the braking/deceleration process. One of the reasons lead to this situation due to the voltage vectors fails to tangentially to the flux vector as the sector used here is the default sector which is not suitable for inverter 100:70 ratio. When the proposed sector is enabled, the deceleration of speed has a better torque regulation and not failed to regulate. Another part to be focused on is the waveform of speed between conventional and proposed sector as the proposed sector has a better speed graph during acceleration and deceleration. The proposed sector allows the ringing/waving effect at the speed measurement.

6. Conclusion

A straightforward approach has been proposed to correct the stator current, stator flux droop, and torque regulation in DTC-OEWIM for medium voltage vectors. The new sector definitions were designed based on the resultant voltage vectors during the mismatched DC-link supply. Moreover, the newly proposed sector definitions optimised the movement of voltage vectors to move in a good circular locus. The main benefit of the proposed method is that it is simple, tunable, and does not add any additional cost to the system. Findings from the research contributed to the advancements of the EV drive application, where under certain circumstances, the supply of the doubly fed inverter may become imbalanced. It provides practical solutions to the existing problems associated with the mismatched operations of the dual inverter system. The research can be further improved by considering the factor of flux linkage for different speed regulation, if the flux linkage reference is not adjusted for each speed, a motor may not reach the desired speed precisely, which could affect the system's overall performance.

Declaration of Competing Interest

The authors declare that they have no known competing financial interests or personal relationships that could have appeared to influence the work reported in this paper.

References

[1] U.R. Muduli, A.R. Beig, R.K. Behera, K.A. Jaafari, J.Y. Alsawalhi, Predictive control with battery power sharing scheme for dual open-end-winding induction motor based four-wheel drive electric vehicle, IEEE Trans. Ind. Electron 69 (6) (June 2022) 5557–5568.

[2] F. Al-Amyal, M. Hamouda, L. Számel, Performance improvement based on adaptive commutation strategy for switched reluctance motors using direct torque control, Alex. Eng. J. 61 (11) (Nov. 2022) 9219–9233, https://doi.org/10.1016/j.aej.2022.02.039.

[3] M.L. De Klerk, A.K. Saha, A comprehensive review of advanced traction motor control techniques suitable for electric vehicle applications, IEEE Access 9 (2021) 125080–125108.

[4] U.R. Muduli, R.K. Behera, K. Al Hosani, M.S.E. Moursi, Direct torque control with constant switching frequency for three-to-five phase direct matrix converter fed five-phase induction motor drive, IEEE Trans. Power Electron., Sept. 37 (9) (2022) 11019–11033.

[5] S.A.A. Tarusan, A. Jidin, M.L.M. Jamil, The optimization of torque ripple reduction by using DTC-multilevel inverter, ISA Trans 121 (Feb. 2022) 365–379.

[6] W. Abd El Maguid Ahmed, M. M. Adel, M. Taha, and A. A. Saleh, "PSO technique applied to sensorless field-oriented control PMSM drive with discretized RL-fractional integral," Alexandria Engineering Journal, vol. 60, no. 4, pp. 4029–4040, Aug. 2021, doi: 10.1016/j.aej.2021.02.049.

[7] A.K. Peter, J. Mathew, K. Gopakumar, A simplified DTC-SVPWM scheme for induction motor drives using a single PI controller, IEEE Trans. Power Electron 38 (1) (Jan. 2023) 750–761.

[8] X. Wu, W. Huang, X. Lin, W. Jiang, Y. Zhao, S. Zhu, Direct torque control for induction motors based on minimum voltage vector error, IEEE Trans. Ind. Electron 68 (5) (May 2021) 3794–3804.

[9] M.H. Holakooie, M. Ojaghi, A. Taheri, Direct torque control of six-phase induction motor with a novel MRAS-based stator resistance estimator, IEEE Trans. Ind. Electron 65 (10) (Oct. 2018) 7685–7696.
[10] I. Takahashi and T. Noguchi, "A New Quick-Response and High-Efficiency Control Strategy of an Induction Motor," *IEEE Trans. Ind. Appl*, vol. IA-22, no. 5, pp. 820–827, 1986.
[11] S.S. Sebtahmadi, H. Pirasteh, S.H. Aghay Kaboli, A. Radan, S. Mekhilef, A 12-sector space vector switching scheme for performance improvement of matrix-converter-based DTC of IM Drive, IEEE Trans. Power Electron 30 (7) (July 2015) 3804–3817.
[12] S. Saleh Hakami, K.B. Lee, Four-level hysteresis-based dtc for torque capability improvement of ipmsm fed by three-level npc inverter, Electronics (Switzerland), Oct. 9 (10) (2020) 1–16.
[13] M.H. Holakooie, G. Iwanski, T. Miazga, Switching-table-based direct torque control of six-phase drives with x−y current regulation, IEEE Trans. Ind. Electron. 69 (12) (Dec. 2022) 11890–11902.
[14] M. Elgbaily, F. Anayi, M.M. Alshbib, A combined control scheme of direct torque control and field-oriented control algorithms for three-phase induction motor: experimental validation, Mathematics 10 (20) (Oct. 2022), https://doi.org/10.3390/math10203842.
[15] S. Krim, S. Gdaim, A. Mtibaa, M.F. Mimouni, Design and implementation of direct torque control based on an intelligent technique of induction motor on FPGA, J. Electr. Eng. Technol. 10 (4) (Jul. 2015) 1527–1539, https://doi.org/10.5370/JEET.2015.10.4.1527.
[16] I.M. Alsofyani, N.R.N. Idris, K.-B. Lee, Dynamic hysteresis torque band for improving the performance of lookup-table-based DTC of induction machines, IEEE Trans. Power Electron 33 (9) (Sept. 2018) 7959–7970.
[17] N.K. Bajjuri, A.K. Jain, An improved dual DTC of double-inverter-fed WRIM drive with reduced torque ripple by emulating equivalent 3L NPC VSC, IEEE Trans. Ind. Electron 69 (6) (June 2022) 5453–5464.
[18] N. el Ouanjli et al, Direct torque control of doubly fed induction motor using three-level NPC inverter, Protection and Control of Modern Power Syst. 4 (1) (Dec. 2019).
[19] S. Lakhimsetty et al, Multilevel torque hysteresis-band based direct-torque control strategy for a three-level open-end winding induction motor drive for electric vehicle applications, IEEE J. Emerging and Selected Topics in Power Electronics 7 (3) (Sept. 2019) 1969–1981.
[20] B.R. Vinod, M.R. Baiju, G. Shiny, Five-level inverter-fed space vector based direct torque control of open-end winding induction motor drive, IEEE Trans. Energy Convers 33 (3) (Sept. 2018) 1392–1401.
[21] M. Salem et al, Improved topology of three-phase series resonant DC-DC boost converter with variable frequency control, Alex. Eng. J. 61 (2) (Feb. 2022) 1701–1713, https://doi.org/10.1016/j.aej.2021.06.078.
[22] H. Hatas, M.N. Almali, Design and control of bypass diode multilevel inverter using a single DC source, Electr. Pow. Syst. Res. 216 (Mar. 2023), https://doi.org/10.1016/J.EPSR.2022.109039 109039.
[23] Z.M.S. El-Barbary, Fuzzy logic based controller for five-phase induction motor drive system, Alex. Eng. J. 51 (4) (2012) 263–268, https://doi.org/10.1016/j.aej.2012.10.005.2.
[24] T. Debnath, K. Gopakumar, L. Umanand, K. Rajashekara, D. Zieliski, "A Generalised multilevel inverter with extended linear modulation range and instantaneously balanced DC-link series capacitors for an induction motor drive," in IEEE, J. Emerging and Selected Topics in Power Electronics (2022), https://doi.org/10.1109/JESTPE.2022.3223096.
[25] M. Es-saadi, H. Chaikhy, M. Khafallah, Implementation and investigation of an advanced induction machine field-oriented control strategy using a new generation of inverters based on dSPACE hardware, Appl. System Innovation 5 (6) (Oct. 2022) 106, https://doi.org/10.3390/asi5060106.
[26] H. A. and J. B., "Scalar and Vector Controlled Infinite Level Inverter (ILI) Topology Fed Open-Ended Three-Phase Induction Motor," in IEEE Access, vol. 9, pp. 98433-98459, 2021, 10.1109/ACCESS.2021.3096125.
[27] V. Jayakumar, B. Chokkalingam, J.L. Munda, A comprehensive review on space vector modulation techniques for neutral point clamped multi-level inverters, IEEE Access 9 (2021) 112104–112144, https://doi.org/10.1109/ACCESS.2021.3100346.
[28] J. Wei, X. Kong, W. Tao, Z. Zhang, B. Zhou, The torque ripple optimization of open-winding permanent magnet synchronous motor with direct torque control strategy over a wide bus voltage ratio range, IEEE Trans. Power Electron 37 (6) (June 2022) 7156–7168.
[29] Y. Luo, C. Liu, A simplified model predictive control for a dual three-phase PMSM With reduced harmonic currents, IEEE Trans. Ind. Electron 65 (11) (Nov. 2018) 9079–9089.
[30] R.E. Kodumur Meesala, V.K. Thippiripati, An improved direct torque control of three-level dual inverter fed open-ended winding induction motor drive based on modified look-up table, IEEE Trans. Power Electron 35 (4) (April 2020) 3906–3917.
[31] K. Kakouche et al, Model predictive direct torque control and fuzzy logic energy management for multi power source electric vehicles, Sensors 22 (15) (Aug. 2022).
[32] A. Oubelaid et al, Secure power management strategy for direct torque controlled fuel cell/ supercapacitor electric vehicles, Front Energy Res 10 (Sep. 2022).
[33] A. Prasanthi, H. Shareef, R. Errouissi, M. Asna, and A. Mohamed, "Hybridization of battery and ultracapacitor for electric vehicle application with dynamic energy management and non-linear state feedback controller," Energy Conversion and Management: X, vol. 15. Elsevier Ltd, Aug. 01, 2022.
[34] G. K. Srinivasan, M. Rivera, V. Loganathan, D. Ravikumar, and B. Mohan, "Trends and challenges in multi-level inverter with reduced switches," Electronics (Switzerland), vol. 10, no. 4. MDPI AG, pp. 1–23, Feb. 02, 2021.
[35] R.B. Jonnala, C. Sai Babu, A modified multiband hysteresis controlled DTC of induction machine with 27-level asymmetrical CHB-MLI with NVC modulation, Ain Shams Eng. J. 9 (1) (Mar. 2018) 15–29, https://doi.org/10.1016/j.asej.2015.08.007.